



Engineering Notes

Feedback Pseudospectral Method for End-of-Life Geostationary Satellites Removal Using Solar Sailing

Hao Mei* and Christopher J. Damaren†

University of Toronto Institute for Aerospace Studies,
Toronto, Ontario M3H 5T6, Canada

and

Xingqun Zhan‡

Shanghai Jiaotong University School of Aeronautics and
Astronautics, 200240 Shanghai, People's Republic of China

<https://doi.org/10.2514/1.G005631>

Nomenclature

A/m	=	area-to-mass ratio of spacecraft, m^2/kg
C_R	=	solar radiation pressure coefficient
\mathcal{F}_g	=	Earth-centered inertial coordinate system
\mathcal{F}_o	=	local-vertical–local-horizontal coordinate system
\mathcal{F}_p	=	perifocal coordinate system
\mathcal{F}_s	=	constructed solar sail coordinate system
\hat{n}	=	normal vector of solar sail
P_\odot	=	characteristic solar radiation pressure, N/m^2
\mathbf{u}	=	control vector
\mathbf{x}	=	state vector
α	=	cone angle of solar sail
δ	=	clock angle of solar sail
μ_3	=	gravitational parameter of the third body, m^3/s
μ_\oplus	=	gravitational parameter of the Earth, m^3/s

Subscripts

sat	=	satellite
\oplus	=	Earth
\odot	=	Sun

I. Introduction

THE increasing population of space debris in the Geostationary Equatorial Orbit (GEO) has been alarming in recent years [1]. The latest annual report “Classification of Geosynchronous Objects” [2] published by the European Space Agency (ESA) indicates that the number of all the known space debris in GEO has been increasing since 2001, and exceeded 1000 in 2018. At present, debris takes up more than 70% of the total object amount. To mitigate the severe situation, the Inter-Agency Space Debris Coordination Committee

(IADC) published the Space Debris Mitigation Guidelines [3] in 2007. According to the guidelines, the GEO protected region should be protected in respect of space debris generation. The GEO protected region ranges from 200 km below the GEO altitude (35,786 km) to 200 km above, and the orbit inclination is restricted within $[-15^\circ, +15^\circ]$. End-of-life GEO satellites should be removed to the GEO graveyard region so as not to interfere with the GEO protected region. To reach the GEO graveyard region, end-of-life GEO satellites should be maneuvered to have a minimal altitude increase of $235 \text{ km} + (1000 \cdot C_R \cdot A/m)$ (C_R and A/m are the solar radiation pressure (SRP) coefficient and the area-to-mass ratio of the spacecraft, respectively), and the terminal orbit eccentricity is restricted within $[0, 0.003]$.

There exists limited research on GEO debris removal using SRP. Reference [4] proposed the TugSat concept, in which a 1000 kg nonfunctional GEO satellite is removed to the GEO graveyard region using an 800 m^2 solar sail. The removal is accomplished by first raising the orbit semi-major axis by 350 km, then reducing the eccentricity to zero. Reference [5] derived an analytical removal solution based on Lyapunov control theory combined with the calculus of variations. In that work, a particle swarm optimizer (PSO) is used to optimize user-designed parameters, which then generates the robust locally time-optimal removal solutions. Reference [6] applied a global Legendre–Gauss–Radau (LGR) pseudospectral (PS) method to find the minimum time solar sailing trajectory for GEO debris removal. In Refs. [4–6], a large area-to-mass ratio (A/m) of spacecraft ($1 \text{ m}^2/kg$) is required to achieve the GEO debris removal. References [7,8] proposed analytical GEO debris removal solutions that required a small A/m of spacecraft (about $0.1 \text{ m}^2/kg$). In Ref. [7], a linear optimal hybrid disturbance accommodation tracking controller was derived to achieve the GEO debris removal using SRP, and the hybrid removal using SRP and impulsive thrusts. Reference [8] proposed an “iterations of linearization” control approach to reduce the terminal state error in [7], and in the meantime achieved the GEO debris removal using realistic solar sails. The terminal state error in [7,8] originates from the inaccuracy of the linearized dynamic systems, whose extent depends on the selection of the nominal state trajectories. In this work, a feedback PS method is proposed and applied to further reduce the terminal state error in [7,8]. In the proposed feedback PS method, the open-loop PS method is used to generate a nominal state trajectory for linearization, and the iterations of the open-loop PS methods and the linear feedback controllers are applied to gradually reduce the inaccuracy of the linearized dynamic systems, thus gradually reducing the terminal state error.

PS methods [9] have been proven very effective in solving nonlinear optimal control problems [10]. The basic idea of this method is to approximate the state and control in terms of their values using a basis of Lagrange polynomials at a finite set of collocation points. Then the time derivative of the state is approximated by differentiating the polynomial approximations of the state and constraining the time derivative to match the vector fields generated by the dynamic system at the collocation points. In this way, optimal control problems are transcribed into nonlinear programming (NLP) problems. The three most commonly used sets of collocation points are the Legendre–Gauss (LG), the Legendre–Gauss–Lobatto (LGL), and the Legendre–Gauss–Radau (LGR) points, which correspond to the LG [11], LGL [12,13], and LGR [14] PS methods, respectively. The comparisons of the LG, LGL, and LGR PS methods can be found in [15,16]. Reference [17] developed a unified framework to investigate the validity of all PS methods in solving optimal control problems, and found that 1) for finite-horizon optimal control problems, the correct PS methods should be based on the Gauss–Lobatto points, 2) for infinite-horizon

Received 28 August 2020; revision received 14 October 2021; accepted for publication 3 November 2021; published online 14 December 2021. Copyright © 2021 by the American Institute of Aeronautics and Astronautics, Inc. All rights reserved. All requests for copying and permission to reprint should be submitted to CCC at www.copyright.com; employ the eISSN 1533-3884 to initiate your request. See also AIAA Rights and Permissions www.aiaa.org/randp.

*Ph.D. Candidate, Spacecraft Dynamics and Control Laboratory, 4925 Dufferin Street; hao.mei@mail.utoronto.ca.

†Professor and Director, 4925 Dufferin Street; damaren@utias.utoronto.ca. Associate Fellow AIAA.

‡Professor and Associate Director, School of Aeronautics and Astronautics, 800 Dongchuan Road; xqzhan@sjtu.edu.cn. Associate Fellow AIAA.

optimal control problems, Gauss–Radau points form the right choice for discretization, and 3) if the wrong PS method is chosen to solve the optimal control problem, suspicion may be cast on the validity of the solution obtained from the wrong PS method. The covector mapping theorems (CMTs) [18,19] showed that one may treat the outcome of the LGL PS method in terms of a rigorous application of the Pontryagin’s minimum principle.

Within the PS methods, there are two different and widely used implementation approaches, namely, the local [20] and global [21] approaches. The global PS methods, where the state and control are parameterized using global polynomials, are known to provide accurate state and control approximations that converge exponentially for problems whose solutions are smooth [10]. In the local PS methods, the time interval is partitioned into several subintervals called segments, and the state and control are parameterized by reasonably low-degree polynomials within each segment. Then the segments are linked via the continuity constraints on the states, and possibly the control. Comparisons of the local and global PS methods can be found in [22,23].

There exists limited literature on feedback PS methods. References [24,25] proposed a real-time feedback PS method using sample-and-hold (SaH) implementation. In this method, the control in the current time interval is generated using PS methods with the sampled states in the previous time interval. Reference [26] used receding horizon control to implement a feedback PS method. The PS method is first used to solve the optimal control problem in the current horizon $[t, t + T]$, then the real-time trajectory in $[t, t + T]$ is obtained using the control given by the PS method, and the real-time state at $t + T$ is fed back as the new initial state for the next horizon $[t + T, t + 2T]$. The procedure is repeated to form receding horizon control. The two existing feedback PS methods, as well as the ordinary open-loop PS methods, are based on the assumption that the applied PS methods generate the globally optimal solutions for nonlinear optimal control problems.

For PS methods to generate the globally optimal solutions, an important condition is that the NLP solvers are able to find the global minima of the transcribed NLP problems. This is exactly the case when the transcribed NLP problems are convex. However, for the nonconvex nonlinear optimal control problems (such as the GEO debris removal problem in this work) whose transcribed NLP problems are nonconvex, NLP solvers may converge to local minima, and this causes the PS methods to generate locally optimal solutions. When locally optimal solutions are generated, the control objectives and desired optimization accuracy may not be achieved. This deficiency is serious because PS methods are open-loop methods. An effective way to solve this problem is to find an effective initial guess that is close to the globally optimal solution and makes the PS methods converge to it. However, for complex nonconvex nonlinear optimal control problems, finding an effective initial guess can be difficult, because the transcribed NLP problems may possess a large number of local minima, and this leads to an open-loop searching process that requires a large computational time. To this end, this Note proposes a feedback PS method in which a linear feedback controller is developed to stabilize the open-loop PS method when it converges to a local minimum.

The main contributions of this Note are as follows. First, we propose a feedback PS method in which a linear feedback controller is developed to stabilize the open-loop PS method when it converges to a local minimum. Second, end-of-life GEO satellites are successfully removed to the GEO graveyard region using solar sailing in conjunction with the proposed feedback PS method, and the terminal state error of the semi-major axis and eccentricity in [7] are reduced from $+13.65$ km to $+0.09$ km, and from $+0.66 \cdot 10^{-3}$ to $-4.09 \cdot 10^{-6}$, respectively.

This Note is organized as follows. Section II presents the dynamic model and the system dynamics for the orbital motion of GEO satellites. Section III describes the proposed feedback PS method, and it is used to remove end-of-life GEO satellites in Sec. IV. Section V draws conclusions.

II. Spacecraft Dynamics and System Modeling

A. Spacecraft Dynamics

This work uses the dynamic model proposed in [7], which is based on the magnitude comparisons of different accelerations exerted on GEO satellites, and the drifts of orbital elements due to each perturbative term over the removal period. The total acceleration exerted on a GEO satellite can be described as $\ddot{\mathbf{r}} = \ddot{\mathbf{r}}_{\oplus} + \ddot{\mathbf{r}}_3 + \ddot{\mathbf{r}}_{\text{SRP}}$. Here, $\ddot{\mathbf{r}}_{\oplus}$ denotes the Earth gravitational acceleration, including the two-body acceleration and Earth gravitational perturbations, $\ddot{\mathbf{r}}_3$ is the third-body (the Sun and Moon) gravitational perturbation, and $\ddot{\mathbf{r}}_{\text{SRP}}$ denotes the acceleration due to SRP. Earth’s gravitational potential is given by ([27] p. 545)

$$U = \frac{\mu_{\oplus}}{r} - \frac{\mu_{\oplus}}{r} \sum_{l=2}^{\infty} J_l \left(\frac{R_{\oplus}}{r} \right)^l P_l[\sin \phi] + \frac{\mu_{\oplus}}{r} \sum_{l=2}^{\infty} \sum_{m=1}^l \left(\frac{R_{\oplus}}{r} \right)^l P_{l,m}[\sin \phi] \{ C_{l,m} \cos(m\lambda_{\text{sat}}) + S_{l,m} \sin(m\lambda_{\text{sat}}) \} \quad (1)$$

Here, μ_{\oplus} is the Earth’s gravitational parameter, r the magnitude of the satellite position vector in the Earth-centered–Earth-fixed (ECEF) frame, ϕ and λ are the latitude and longitude of satellite, P_l ($P_{l,m}$) denotes the conventional (associated) Legendre polynomials, and J_l ($C_{l,m}$, $S_{l,m}$) are the zonal (sectoral and tesseral) harmonics. Earth’s gravitational acceleration in the ECEF frame can be obtained by taking the gradient of the total gravitational potential. As in [7], this work applies the second- and the third-order terms of the Earth’s gravitational perturbation in the dynamic model.

The equation of motion of a three-body system is given by ([27] p. 574)

$$\ddot{\mathbf{r}}_{\oplus\text{sat}} = -\frac{\mu_{\oplus} \mathbf{r}_{\oplus\text{sat}}}{r_{\oplus\text{sat}}^3} + \mu_3 \left(\frac{\mathbf{r}_{\text{sat}3}}{r_{\text{sat}3}^3} - \frac{\mathbf{r}_{\oplus 3}}{r_{\oplus 3}^3} \right) \quad (2)$$

Here μ_3 is the gravitational parameter of the third body. By expanding the term $\mathbf{r}_{\text{sat}3}/r_{\text{sat}3}^3$ in Eq. (2) using Legendre polynomials, Eq. (2) becomes

$$\ddot{\mathbf{r}}_{\oplus\text{sat}} = -\frac{\mu_{\oplus} \mathbf{r}_{\oplus\text{sat}}}{r_{\oplus\text{sat}}^3} - \mu_3 \left(\frac{-\mathbf{r}_{\text{sat}3}(3B + 3B^2 + B^3) + \mathbf{r}_{\oplus 3}}{r_{\oplus 3}^3} \right) \quad (3)$$

$$B = \sum_{j=1}^{\infty} P_j[\cos \zeta] \left(\frac{r_{\oplus\text{sat}}}{r_{\oplus 3}} \right)^j \quad (4)$$

Here ζ is the angle between $\mathbf{r}_{\oplus 3}$ and $\mathbf{r}_{\oplus\text{sat}}$. Equation (4) can be partitioned as $B = B_1 + B_2 + B_3 + \dots$. As in [7], this work uses the following dynamic model for the third-body gravitational accelerations. For the Sun, the B_1 and B_2 terms are applied. For the Moon, the B_1 , B_2 , and B_3 terms are considered when $A/m \geq 0.1$ m²/kg, whereas the B_4 and B_5 terms are also taken into consideration when $A/m \geq 0.001$ m²/kg.

The acceleration caused by SRP for a perfectly reflecting solar sail is given by ([28] p. 39)

$$\ddot{\mathbf{r}}_{\text{SRP}} = \left(2P_{\odot} \frac{A}{m} \cos^2 \alpha \right) \hat{\mathbf{n}} \quad (5)$$

Here P_{\odot} denotes the magnitude of SRP that at 1 AU from the Sun is equal to 4.56×10^{-6} N/m². A/m is the area-to-mass ratio of spacecraft, and α denotes the cone angle (the pitch angle in the 2D case) of the solar sail, which is the angle between the sail normal vector $\hat{\mathbf{n}}$ and

the sun-line vector $\hat{\mathbf{u}}$. A GEO satellite experiences eclipse by the Earth in the summer and winter. This works applies the cylindrical eclipse shadow model, which is detailed in [7].

B. System Modeling

This work takes the classical orbital elements $\mathbf{x} = [a, e, i, \omega, \Omega, \theta]$ as the state. The classical orbital elements exhibit singularities in GEO. When the inclination i and eccentricity e reach zero, the argument of perigee ω and right ascension of ascending node (RAAN) Ω are not defined. However, the orbital elements that are to be maneuvered (semi-major axis, eccentricity, and inclination) are well-defined in GEO. We can set the initial inclination and eccentricity to small numbers (but not zero) to avoid numerical difficulties in the orbit propagation. The time derivative of the state is given by ([27] p. 636)

$$\frac{d}{dt} \underbrace{\begin{pmatrix} a \\ e \\ i \\ \omega \\ \Omega \\ \theta \end{pmatrix}}_{\mathbf{x}} = \underbrace{\begin{pmatrix} \frac{2a^2}{\sqrt{\mu_{\oplus} a(1-e^2)}} e \sin(\theta) & \frac{2a^2}{\sqrt{\mu_{\oplus} a(1-e^2)}} (1+e \cos(\theta)) & 0 & 0 & 0 & 0 \\ \sqrt{\frac{a(1-e^2)}{\mu_{\oplus}}} \sin(\theta) & \sqrt{\frac{a(1-e^2)}{\mu_{\oplus}}} \frac{2 \cos(\theta) + e(1+\cos^2(\theta))}{1+e \cos(\theta)} & 0 & 0 & 0 & 0 \\ 0 & 0 & \sqrt{\frac{a(1-e^2)}{\mu_{\oplus}}} \frac{\cos(\omega+\theta)}{1+e \cos(\theta)} & -\sqrt{\frac{a(1-e^2)}{\mu_{\oplus}}} \frac{\sin(\omega+\theta)}{\tan(i)(1+e \cos(\theta))} & \sqrt{\frac{\mu_{\oplus}}{a^3}} \frac{(1+e \cos(\theta))^2}{\sqrt{(1-e^2)^3}} & 0 \\ -\sqrt{\frac{a(1-e^2)}{\mu_{\oplus}}} \frac{\cos(\theta)}{e} & \sqrt{\frac{a(1-e^2)}{\mu_{\oplus}}} \frac{(2+e \cos(\theta)) \sin(\theta)}{e(1+e \cos(\theta))} & -\sqrt{\frac{a(1-e^2)}{\mu_{\oplus}}} \frac{\sin(\omega+\theta)}{\tan(i)(1+e \cos(\theta))} & \sqrt{\frac{a(1-e^2)}{\mu_{\oplus}}} \frac{\sin(\omega+\theta)}{\sin(i)(1+e \cos(\theta))} & 0 & 0 \\ 0 & 0 & \sqrt{\frac{a(1-e^2)}{\mu_{\oplus}}} \frac{\cos(\theta)}{e} & -\sqrt{\frac{a(1-e^2)}{\mu_{\oplus}}} \frac{(2+e \cos(\theta)) \sin(\theta)}{e(1+e \cos(\theta))} & 0 & 0 \\ \sqrt{\frac{a(1-e^2)}{\mu_{\oplus}}} \frac{\cos(\theta)}{e} & -\sqrt{\frac{a(1-e^2)}{\mu_{\oplus}}} \frac{(2+e \cos(\theta)) \sin(\theta)}{e(1+e \cos(\theta))} & 0 & 0 & 0 & 0 \end{pmatrix}}_{\text{denote as } P(\mathbf{x})} \begin{pmatrix} f_r \\ f_\theta \\ f_z \end{pmatrix} + \underbrace{\begin{pmatrix} 0 \\ 0 \\ 0 \\ 0 \\ 0 \\ \sqrt{\frac{\mu_{\oplus}}{a^3}} \frac{(1+e \cos(\theta))^2}{\sqrt{(1-e^2)^3}} \end{pmatrix}}_{\text{denote as } \mathbf{b}(\mathbf{x})} \quad (6)$$

Here f_r, f_θ, f_z denote the perturbative forces in the local-vertical–local-horizontal (LVLH, denoted as \mathcal{F}_o) frame.

To express the acceleration due to SRP, a new frame \mathcal{F}_s is constructed. As depicted in Fig. 1a, axis $\hat{\mathbf{s}}_1$ is aligned with the sun-line vector $\hat{\mathbf{u}}$ (points from the Sun to the satellite), axis $\hat{\mathbf{s}}_3$ lies in the plane constructed by $\hat{\mathbf{s}}_1$ and $\hat{\mathbf{g}}_3$ and being perpendicular to $\hat{\mathbf{s}}_1$, and axis $\hat{\mathbf{s}}_2$ completes the right-hand rule.

The sail normal vector $\hat{\mathbf{n}}$ in \mathcal{F}_s is given by $\mathbf{n}_s = [\cos \alpha, \sin(\alpha) \sin(\delta), \sin(\alpha) \cos(\delta)]^T$, where α ($\in [0^\circ, 90^\circ]$) and δ ($\in [0^\circ, 360^\circ]$) are the cone angle and clock angle of the sail (Fig. 1b). The rotation matrix from \mathcal{F}_s to \mathcal{F}_g is given by $\mathbf{C}_{GS} = \mathbf{f}_g \cdot \mathbf{f}_s^T$, in which \mathbf{f}_g defines the vectrix denoted as $\mathbf{f}_g = (\hat{\mathbf{g}}_1, \hat{\mathbf{g}}_2, \hat{\mathbf{g}}_3)^T$ and similarly $\mathbf{f}_s = (\hat{\mathbf{s}}_1, \hat{\mathbf{s}}_2, \hat{\mathbf{s}}_3)^T$. Recall that the acceleration due to SRP for an ideal solar sail is equal to $2P_{\odot} \cdot (A/m) \cdot \cos^2(\alpha) \cdot \hat{\mathbf{n}}$; thus the acceleration due to SRP in the LVLH frame (\mathcal{F}_o) can be expressed as $2P_{\odot} \cdot A/m \cdot \cos^2(\alpha) \cdot \mathbf{C}_{OP} \mathbf{C}_{PG} \mathbf{C}_{GS} \cdot \mathbf{n}_s$. Here $\mathbf{C}_{OP} = \mathbf{C}_3(\theta)$, $\mathbf{C}_{PG} = \mathbf{C}_3(\omega) \mathbf{C}_1(i) \mathbf{C}_3(\Omega)$ are rotation matrices from the perifocal coordinate frame (denoted as \mathcal{F}_p) to \mathcal{F}_o and from \mathcal{F}_g to \mathcal{F}_p , respectively. Taking the disturbances into account, we have

$$\dot{\mathbf{x}}(t) \triangleq \mathbf{f}_c(\mathbf{x}, \mathbf{u}, t) = \mathbf{f}_{\text{SRP}}(\mathbf{x}, \mathbf{u}, t) + \mathbf{d}(t) \quad (7)$$

Here $\mathbf{f}_{\text{SRP}}(\mathbf{x}, \mathbf{u}, t) = 2P_{\odot} \cdot (A/m) \cdot \cos^2(\alpha) \cdot \mathbf{P}(\mathbf{x}) \cdot \mathbf{C}_{OP} \mathbf{C}_{PG} \mathbf{C}_{GS} \cdot \mathbf{n}_s + \mathbf{b}(\mathbf{x})$ defines the time derivative of the state due to SRP, in which \mathbf{n}_s is determined by the control angles α and δ . The term $\mathbf{d}(t) = \mathbf{P}(\mathbf{x}(t)) \cdot \mathbf{a}_d(t)$ denotes the disturbance, where $\mathbf{a}_d(t)$ is the perturbative accel-

eration expressed in \mathcal{F}_o . Note that in this work the disturbance is approximated and modeled as a function only of time.

III. Feedback Pseudospectral Method

A. General Description

The convergence of the PS methods depends on the initial guesses, especially when solving nonconvex nonlinear optimal control problems. An effective initial guess makes the PS method converge to the global minimum, whereas an ineffective initial guess causes the PS method to converge to a local minimum. When the local minima are reached, the control objectives and the desired optimization accuracy may not be achieved. For complex nonconvex nonlinear optimal control problems, finding an effective initial guess can be difficult, because the transcribed NLP problems may possess a large number of local minima, and the open-loop searching process could cost a large

computational time. This deficiency is serious because PS methods are open-loop methods. This work applies feedback approaches to counter this deficiency.

As shown in Fig. 2, when the initial guess is ineffective, the open-loop PS method first converges to a local minimum. Then we linearize the dynamic system along the locally optimal state trajectory and design a linear feedback controller to further reduce the cost function. The penalty matrices in the linear feedback controller can be chosen based on trial and error. The real-time control is the addition of the feedforward control generated by the open-loop PS method, and the feedback control obtained from the linear feedback controller.

Furthermore, the real-time state trajectory obtained from the linear feedback controller deviates from the nominal trajectory along which the dynamic system is linearized, and this causes error in the linearized dynamic system, which further causes terminal state error. This work proposes two iterative approaches to gradually reduce the inaccuracy of the linearized dynamic systems, thus gradually reducing the terminal state error. In the iterative approach I, the dynamic system is linearized along the real-time state trajectory generated by the linear feedback controller in the last iteration, and another linear feedback controller is applied to further reduce the cost function. The penalty matrices in the linear feedback controllers can be chosen based on trial and error. In the iterative approach II, the real-time control and state trajectory act as the initial guesses for the open-loop PS method in the next iteration, and another linear feedback controller is applied to stabilize the open-loop PS method. During the iterations, the bounds on the states can be shrunk in each step of the

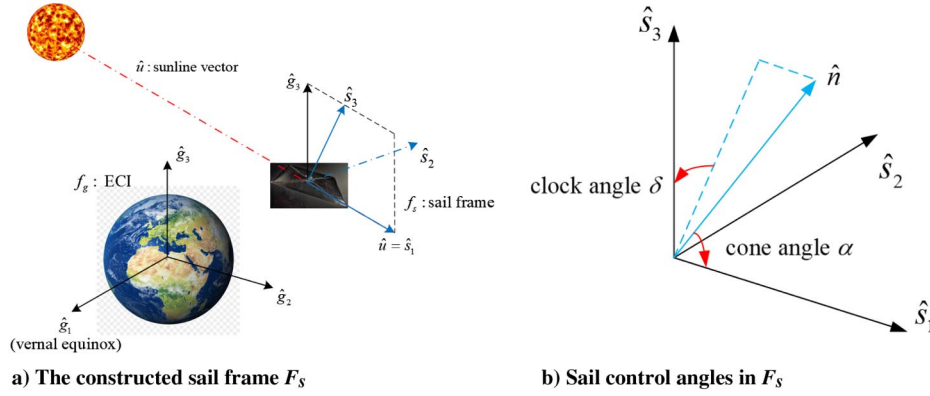


Fig. 1 The solar sail frame and control angles.

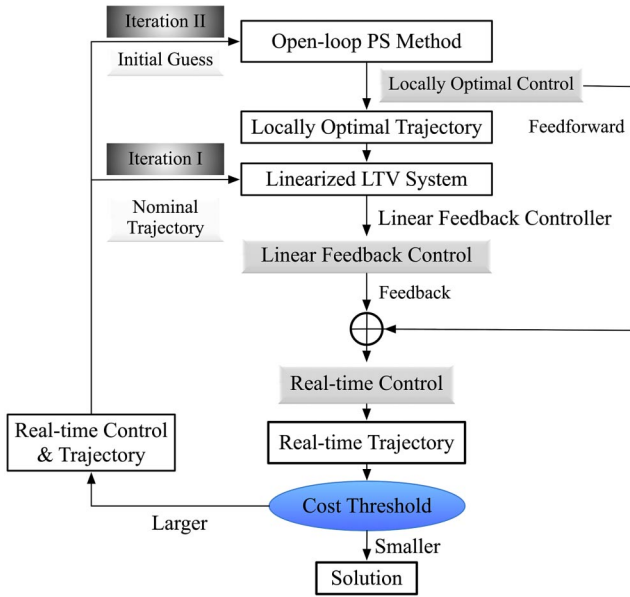


Fig. 2 General description of the feedback pseudospectral method.

open-loop PS optimization, and the penalty matrices in the linear feedback controllers can be chosen based on trial and error. Figure 2 illustrates the proposed feedback PS method and is summarized as follows:

- 1) The locally optimal state trajectory generated by the open-loop PS method acts as a nominal trajectory. Then the dynamic system is linearized along the nominal trajectory.
- 2) Based on the linearized system in step 1), a linear feedback controller is developed to further reduce the cost function.
- 3) The real-time control is the addition of the feedforward control generated by the open-loop PS method and the feedback control obtained from the linear feedback controller.
- 4) In the iterative approach I, the dynamic system is linearized along the real-time state trajectory generated by the linear feedback controller in the last iteration, and another linear feedback controller is applied to further reduce the cost function. The penalty matrices in the linear feedback controllers can be chosen based on trial and error.
- 5) In the iterative approach II, the real-time control and state trajectory act as the initial guesses for the open-loop PS method in the next iteration, and another linear feedback controller is applied to stabilize the open-loop PS method. During the iterations, the bounds on the states can be shrunk in each step of the open-loop PS optimization, and the penalty matrices in the linear feedback controllers can be chosen based on trial and error.

6) The solution is generated when the cost value is smaller than the cost threshold, and it is given by the real-time control and state trajectory generated by the last iteration.

B. Legendre–Gauss–Lobatto (Open-Loop) Pseudospectral Method

A general continuous optimal control problem is formulated as follows. Determine the state-control pair $\{x \in \mathbb{R}^{N_x}, u \in \mathbb{R}^{N_u}\}$ that minimizes the Bolza form cost functional:

$$\mathcal{J} = \phi[x(t_f), t_f] + \int_{t_0}^{t_f} \mathcal{L}(x(t), u(t), t) dt \quad (8)$$

subject to

$$\dot{x}(t) = f(x(t), u(t), t) \quad (9)$$

$$C(x, u, t) = 0 \quad (10)$$

$$H(x, u, t) \leq 0 \quad (11)$$

$$E(x(t_0), x(t_f), t_0, t_f) = 0 \quad (12)$$

where $f: \mathbb{R}^{N_x} \times \mathbb{R}^{N_u} \times \mathbb{R} \rightarrow \mathbb{R}^{N_x}$ is the system dynamic constraint; $C: \mathbb{R}^{N_x} \times \mathbb{R}^{N_u} \times \mathbb{R} \rightarrow \mathbb{R}^{N_c}$ and $H: \mathbb{R}^{N_x} \times \mathbb{R}^{N_u} \times \mathbb{R} \rightarrow \mathbb{R}^{N_h}$ are the equality and inequality constraints, respectively; and $E: \mathbb{R}^{N_x} \times \mathbb{R}^{N_x} \times \mathbb{R} \times \mathbb{R} \rightarrow \mathbb{R}^{N_e}$ denotes the boundary conditions. The optimal control problem can be transformed into an NLP problem using the LGL PS method. The basic idea of this method is to approximate the state and control using polynomials that interpolate their values at the LGL points.

The $N + 1$ LGL points $(t_i, i = 0, \dots, N)$ are distributed over the interval $[-1, 1]$ and are given by $t_0 = -1$, $t_N = 1$, and $t_l (1 \leq l \leq N - 1)$ are the zeros of \dot{L}_N . First the problem is transformed from $t = [t_0, t_f]$ into $\tau = [-1, 1]$ using

$$\tau = \frac{2t}{t_f - t_0} - \frac{t_f + t_0}{t_f - t_0} \quad (13)$$

Then the state and control are approximated using the Lagrange basis polynomials $L_i(\tau)$:

$$x(\tau) = \sum_{i=0}^N X_i L_i(\tau) \quad (14)$$

$$u(\tau) = \sum_{i=0}^N U_i L_i(\tau) \quad (15)$$

where X_i and U_i are the coordinates of the state and control under the basis $L_i(\tau)$.

Differentiating Eq. (14) and evaluating at the k th collocation point results in

$$\dot{\mathbf{x}}(\tau_k) = \sum_{i=0}^N X_i \dot{L}_i(\tau_k) = \sum_{i=0}^N D_{ki} X_i(\tau_k) \quad (16)$$

The state derivatives at the collocation points should match the local vector fields imposed by Eq. (9); thus

$$D\mathbf{X}_{0:N} = \left(\frac{t_f - t_0}{2} \right) \mathbf{F}(\mathbf{X}_{0:N}, \mathbf{U}_{0:N}, t(\tau_{0:N})) \quad (17)$$

where the $(N+1) \times (N+1)$ square matrix \mathbf{D} is the Lobatto PS differentiation matrix.

Now the NLP problem obtained from transcribing the optimal control problem given by Eqs. (8–12) can be written in the following manner. Minimize

$$\mathcal{J} = \phi[\mathbf{X}_N, t_f] + \left(\frac{t_f - t_0}{2} \right) \sum_{i=0}^N \omega_i \mathcal{L}(\mathbf{X}_i, \mathbf{U}_i, t(\tau_i)) \quad (18)$$

subject to

$$D\mathbf{X}_{0:N} - \left(\frac{t_f - t_0}{2} \right) \mathbf{F}(\mathbf{X}_{0:N}, \mathbf{U}_{0:N}, t(\tau_{0:N})) = \mathbf{0} \quad (19)$$

$$\mathbf{C}(\mathbf{X}_{0:N}, \mathbf{U}_{0:N}, t(\tau_{0:N})) = \mathbf{0} \quad (20)$$

$$\mathbf{H}(\mathbf{X}_{0:N}, \mathbf{U}_{0:N}, t(\tau_{0:N})) \leq \mathbf{0} \quad (21)$$

$$\mathbf{E}(\mathbf{X}_0, \mathbf{X}_N, t_0, t_f) = \mathbf{0} \quad (22)$$

where $\omega_i (i = 0, 1, \dots, N)$ in Eq. (18) are the LGL weights and are given as

$$\omega_i = \frac{2}{N(N+1)} \frac{1}{[L_N(t_i)]^2}, \quad i = 0, 1, \dots, N \quad (23)$$

C. Linear Feedback Controller

Consider the dynamic system in Eq. (7), $\dot{\mathbf{x}}(t) = \mathbf{g}(\mathbf{x}(t), \mathbf{u}(t), t)$, where $\mathbf{u} = [\alpha, \delta]^T$. By linearizing the dynamic system along the nominal trajectory $\{\mathbf{x}_n(t), \mathbf{u}_n(t), \mathbf{d}_n(t)\}$ generated by the open-loop PS method in Sec. III.B, we have

$$\dot{\mathbf{x}}(t) = \dot{\mathbf{x}}_n(t) + (\delta\dot{\mathbf{x}})(t) \quad (24)$$

$$\dot{\mathbf{x}}_n(t) = \mathbf{g}(\mathbf{x}_n(t), \mathbf{u}_n(t), t) \quad (25)$$

$$\dot{\mathbf{x}}(t) = \mathbf{g}(\mathbf{x}_n(t), \mathbf{u}_n(t), t) + \frac{\partial \mathbf{g}}{\partial \mathbf{x}}[\mathbf{x}_n, \mathbf{u}_n, t] \delta \mathbf{x}(t) + \frac{\partial \mathbf{g}}{\partial \mathbf{u}}[\mathbf{x}_n, \mathbf{u}_n, t] \delta \mathbf{u}(t) \quad (26)$$

which result in

$$(\delta\dot{\mathbf{x}})(t) = \underbrace{\frac{\partial \mathbf{g}}{\partial \mathbf{x}}[\mathbf{x}_n, \mathbf{u}_n, t] \delta \mathbf{x}(t)}_{\text{denote as } \mathbf{A}(t)} + \underbrace{\frac{\partial \mathbf{g}}{\partial \mathbf{u}}[\mathbf{x}_n, \mathbf{u}_n, t] \delta \mathbf{u}(t)}_{\text{denote as } \mathbf{B}(t)} \quad (27)$$

Here $\delta \mathbf{x}(t) = \mathbf{x}(t) - \mathbf{x}_n(t)$ and $\delta \mathbf{u}(t) = \mathbf{u}(t) - \mathbf{u}_n(t)$ are deviations from the nominal trajectory and nominal control input, respectively. With $\mathbf{X} \triangleq \delta \mathbf{x}$ and $\mathbf{U} \triangleq \delta \mathbf{u}$, Eq. (27) becomes

$$\dot{\mathbf{X}}(t) = \mathbf{A}(t)\mathbf{X}(t) + \mathbf{B}(t)\mathbf{U}(t) \quad (28)$$

This is a linear time varying (LTV) system, where $\mathbf{A}(t)$ and $\mathbf{B}(t)$ are modeled along the nominal trajectory $\{\mathbf{x}_n(t), \mathbf{u}_n(t), \mathbf{d}_n(t)\}$.

If the state $\mathbf{X}(t) = \mathbf{x}(t) - \mathbf{x}_n(t)$ in the linearized system (Eq. (28)) tracks the desired trajectory $\mathbf{Z}(t)$ defined as $\mathbf{x}_d(t) - \mathbf{x}_n(t)$, then $\mathbf{x}(t) = \mathbf{x}_d(t)$, which is the desired situation. Therefore, it turns out to be a tracking problem ([29] Sec. 6). We seek to minimize the cost functional

$$\begin{aligned} \mathcal{J}(\mathbf{X}(t), \mathbf{Z}(t), \mathbf{U}(t)) = & \frac{1}{2} \mathbf{e}^T(t_f) \mathbf{S} \mathbf{e}(t_f) + \int_{t_0}^{t_f} \left(\frac{1}{2} \mathbf{e}^T(t) \mathbf{Q} \mathbf{e}(t) \right. \\ & \left. + \frac{1}{2} \mathbf{U}^T(t) \mathbf{R} \mathbf{U}(t) \right) dt \end{aligned} \quad (29)$$

where $\mathbf{e}(t) = \mathbf{X}(t) - \mathbf{Z}(t)$ denotes the tracking error. The matrix $\mathbf{S} = \mathbf{S}^T \geq 0$ penalizes the terminal tracking error, $\mathbf{Q} = \mathbf{Q}^T \geq 0$ penalizes the tracking error, and $\mathbf{R} = \mathbf{R}^T > 0$ penalizes the control inputs. The solution of this problem can be obtained from Eq. (51) in [7] by setting the disturbance term to zero, and it is given by

$$\mathbf{U}^*(t) = -\mathbf{R}^{-1} \mathbf{B}^T(t) (\mathbf{P}(t) \mathbf{X}(t) - \mathbf{g}(t)) \quad (30)$$

where $\mathbf{P}(t)$ and $\mathbf{g}(t)$ can be calculated by integrating the following equations simultaneously backward:

$$\dot{\mathbf{P}}(t) = -\mathbf{Q} - \mathbf{A}^T(t) \mathbf{P}(t) - \mathbf{P}(t) \mathbf{A}(t) + \mathbf{P}(t) \mathbf{B}(t) \mathbf{R}^{-1} \mathbf{B}^T(t) \mathbf{P}(t) \quad (31)$$

$$\dot{\mathbf{g}}(t) = -\mathbf{Q} \mathbf{Z}(t) - (\mathbf{A}^T(t) - \mathbf{P}(t) \mathbf{B}(t) \mathbf{R}^{-1} \mathbf{B}^T(t)) \mathbf{g}(t) \quad (32)$$

using the boundary conditions

$$\mathbf{P}(t_f) = \mathbf{S} \quad (33)$$

$$\mathbf{g}(t_f) = \mathbf{S} \mathbf{Z}(t_f) \quad (34)$$

D. Real-Time Control

The real-time control is given by

$$\mathbf{u}_{\text{realtime}} = \mathbf{u}_{\text{feedforward}} + \mathbf{u}_{\text{feedback}} \quad (35)$$

Here $\mathbf{u}_{\text{feedforward}}$ is generated by the open-loop PS method in Sec. III.B and $\mathbf{u}_{\text{feedback}}$ is obtained from the linear feedback controller in Sec. III.C and given by Eq. (30).

IV. End-of-Life GEO Satellites Removal

The control objective is to raise the orbit semi-major axis by 305 km and make the terminal eccentricity smaller than 10^{-4} . In this way, the terminal perigee will be raised slightly more than 300 km and the terminal orbit will be placed in the GEO graveyard region. To avoid the singularity of the classical orbital elements, the desired eccentricity of the terminal orbit is set to be a small but nonzero number (10^{-4}).

The initial position of the satellite in the ECI frame is set to be [0.0 m, 42,164.8 km, 1.0 m]. The initial time is Jan 1st, 2017, 00:00:00, with the time constants $\Delta \text{UT}(\text{UT1} - \text{UTC}) = 0.359485$ s and $\Delta \text{AT}(\text{TAI} - \text{UTC}) = 37.0$ s. The terminal time $t_f = 350$ days. The A/m of the spacecraft is equal to 0.14 m²/kg. The real-time state trajectory is propagated using the fourth-order Runge–Kutta method (RK4), and the time step is set to be 30 s.

A. Optimization Using the LGL Pseudospectral (Open-Loop) Method

a) Formulation and setup

We seek to minimize

$$\mathcal{J} = (|a_{t_f} - a_d|, |e_{t_f} - e_d|) \cdot \mathbf{S}_{ol} \quad (36)$$

subject to

$$\begin{aligned} \dot{\mathbf{x}}(t) &= \mathbf{g}(\mathbf{x}(t), \mathbf{u}(t), \mathbf{d}(t)) \\ [42164 - 10 \text{ km}, 0, 0, 0, 0, 0]^T &\leq \mathbf{x} \leq \\ &\times \left[42164 + 350 \text{ km}, 0.1, \frac{\pi}{180}, 3\pi, 2\pi, 700\pi \right]^T \\ [0, 0]^T &\leq \mathbf{u} \leq \left[\frac{\pi}{2}, 2\pi \right]^T \\ \mathbf{x}(t_0) &= \mathbf{x}_0 \end{aligned} \quad (37)$$

Here $a_d = 42164 \text{ km} + 305 \text{ km} = 42469 \text{ km}$ and $e_d = 10^{-4}$ are the desired semi-major axis and eccentricity, respectively. The dynamic equation is given in Eq. (7). A local LGL PS method is used to transform the optimal control problem into an NLP problem. The initial guesses for the states and control are given by the nominal trajectory in [7]. In the nominal trajectory, the argument of perigee and RAAN show oscillations in the first 20 days, during which the local LGL PS method shows poor convergence. Thus in this work, the first 20 days are cut off, and the real-time state at the end of the 20th day acts as the initial state for the local LGL PS optimization. The resulting initial guesses for the remaining 330 days are presented in Fig. 3. In the initial guess, the terminal state error of the semi-major axis and eccentricity are $+26.6954 \text{ km}$ and $+4.0415 \cdot 10^{-4}$, respectively.

In the initial guess, the cone angle α is equal to 0° when the satellite moves away from the Sun, and 90° when moves toward the Sun. Each of the 0 and 90° periods lasts about half an orbit (about 12 h for a GEO satellite). To make the polynomial approximation of the cone angle α as accurate as possible, the segment boundaries of the local LGL PS method are chosen to be the first epochs of the 0 and 90° periods. In this way, each segment in the local LGL PS method corresponds to a single 0 or 90° period of the cone angle α .

b) Implementation using receding horizon control

The local LGL PS optimization is implemented using receding horizon control, which is detailed in [26]. The real-time state at the end of the current horizon acts as the initial state for the local LGL PS optimization in the next horizon. In this work, the horizon is set to be

one sidereal day. The optimization goal of each horizon day is to reduce the terminal semi-major axis and eccentricity error in the initial guess by a portion of $1/330$ (80.89 m and $1.22 \cdot 10^{-6}$ for semi-major axis and eccentricity, respectively). The removal time is 330 days. For each horizon day, the desired semi-major axis $a_{\text{dhor}} = [(42164.8 + 305) \cdot 10^3 + 26695.4 - k \cdot 80.89] \text{ m}$, the desired eccentricity $e_{\text{dhor}} = 1 \cdot 10^{-4} + 4.04 \cdot 10^{-4} - k \cdot 1.22 \cdot 10^{-6}$, and $k = 1, 2, \dots, 330$ is the number of the horizon day. For each segment in the local LGL PS method, 20 collocation points are applied. The penalty matrix in Eq. (36) is set to be $S_{ol} = [10^{-3}, 10^5]^T$. The transcribed NLP problem is solved using SNOPT [30], and the major optimality/feasibility tolerance in SNOPT is set to be 10^{-5} . On each horizon day, the bounds on the states are set to be a little higher (lower) than the maximum (minimum) value of the initial guesses. Figure 4 presents the optimization results of the first horizon day.

The real-time state at the end of the first horizon day acts as the initial state for the local LGL PS optimization in the second horizon day. Repeating this process to form receding horizon control, the real-time control and state trajectory for the whole removal time (330 days) are presented in Fig. 5. Figures 5e and 5f show the tracking error of the semi-major axis and eccentricity at the end of each horizon day, from which we can see that the semi-major axis and eccentricity tracking error grow with time. This is because the trajectories of the initial guesses deviate from the real-time state trajectories as the tracking error accumulates. Using the local LGL PS method, the terminal state error of the semi-major axis and eccentricity are reduced from $+26.6954$ to $+11.1413 \text{ km}$, and from $+4.0415 \cdot 10^{-4}$ to $+1.6025 \cdot 10^{-4}$, respectively, and the cost is also reduced from 67.1094 to 27.1663. The maximal rate of change of the control angles is about 16 deg per minute.

B. Optimization Using the Feedback PS Method

Now we linearize the dynamic system given in Eq. (7) along the locally optimal state trajectory generated by the local LGL PS method, and apply the linear feedback controller developed in Sec. III.C to further reduce the cost function. The real-time control

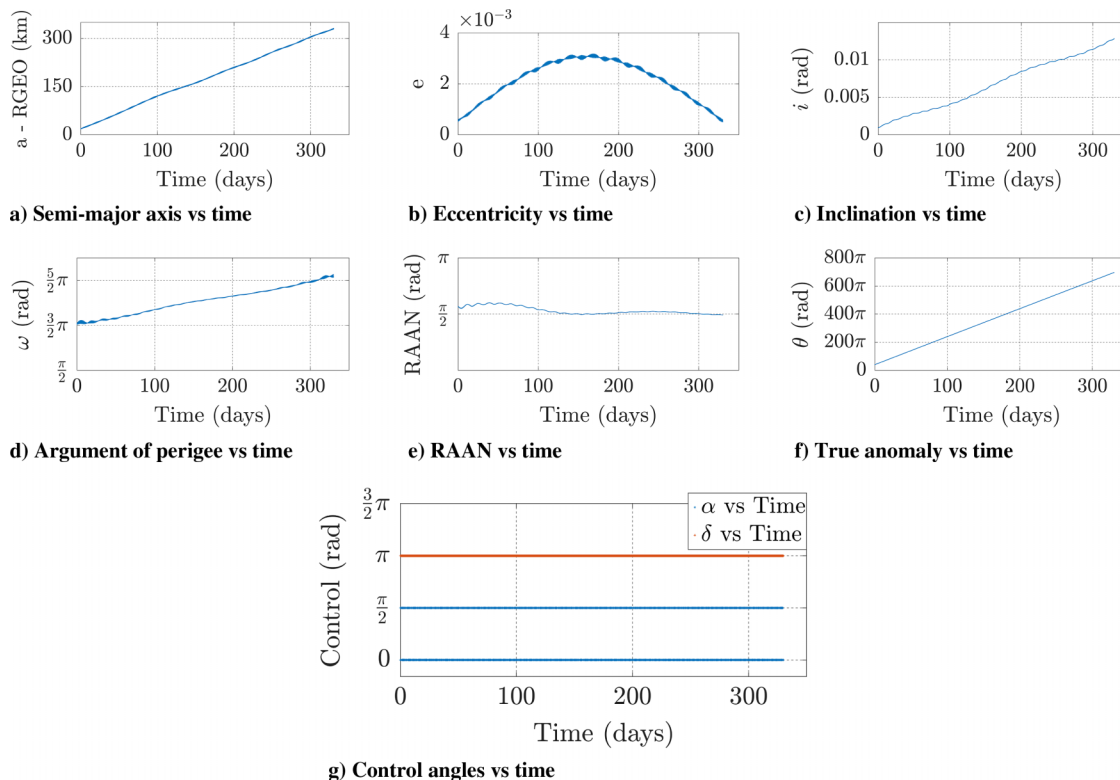


Fig. 3 The initial guesses for the states and control angles.

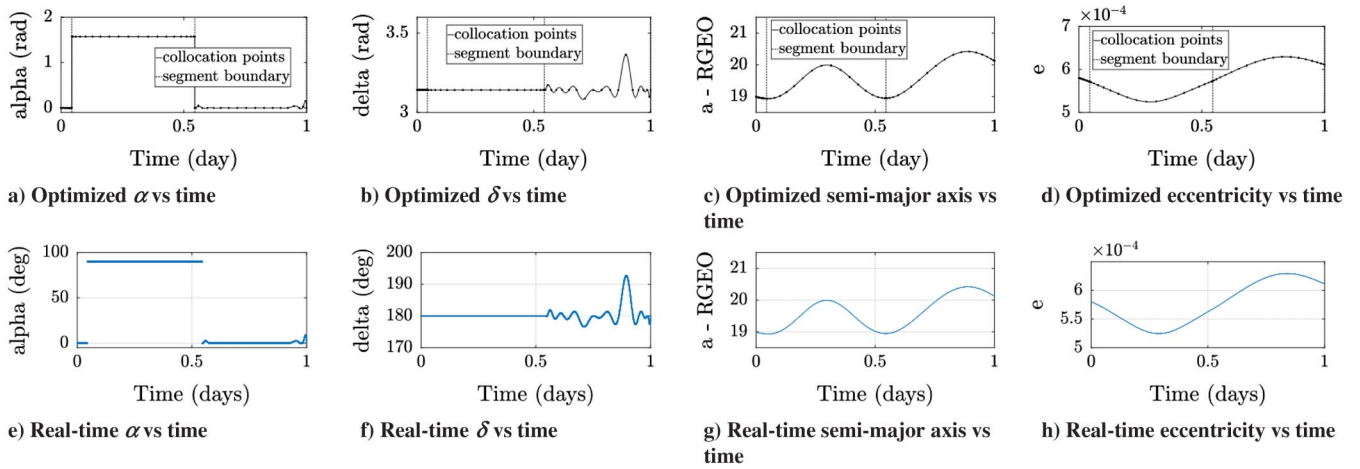


Fig. 4 Optimization using the local LGL PS method on the first horizon day.

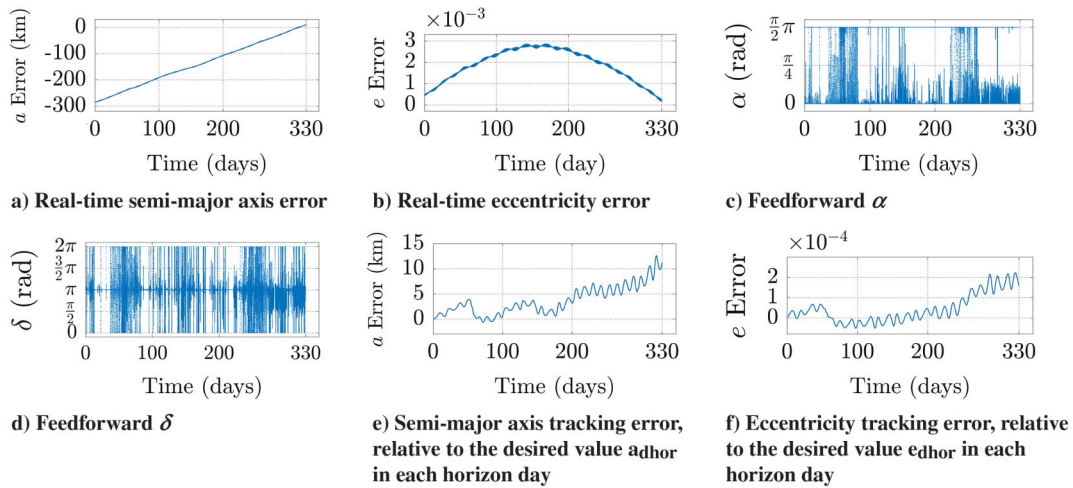


Fig. 5 The real-time states and control angles for the whole removal time (330 days), optimization using the local LGL PS method.

is given by $\mathbf{u}_{\text{realtime}} = \mathbf{u}_{\text{feedforward}} + \mathbf{u}_{\text{feedback}}$, where $\mathbf{u}_{\text{feedforward}}$ is generated by the open-loop PS method presented in Fig. 5, and $\mathbf{u}_{\text{feedback}}$ is obtained from the linear feedback controller and given by Eq. (30). The penalty matrices in Eq. (29) are set to be $\mathbf{S} = \text{diag}[10, 10^{10}, 1, 1, 1, 1]$, $\mathbf{Q} = \text{diag}[10, 10^6, 1, 1, 1, 1]$, $\mathbf{R} = \text{diag}[10^{14}, 10^{14}]$. The feedback and real-time control, along with the real-time state trajectory, are presented in Fig. 6. The terminal state error of the semi-major axis and eccentricity are reduced from +11.1413 to

+7.5692 km, and from $+1.6025 \cdot 10^{-4}$ to $+5.7399 \cdot 10^{-5}$, respectively, and the cost is reduced from 27.1663 to 13.3091.

The real-time state trajectory deviates from the nominal trajectory along which the dynamic system is linearized, and this causes error in the LTV system, which further causes terminal state error. Here we apply two iterative approaches to gradually reduce the inaccuracy of the LTV systems, thus gradually reducing the terminal state error.

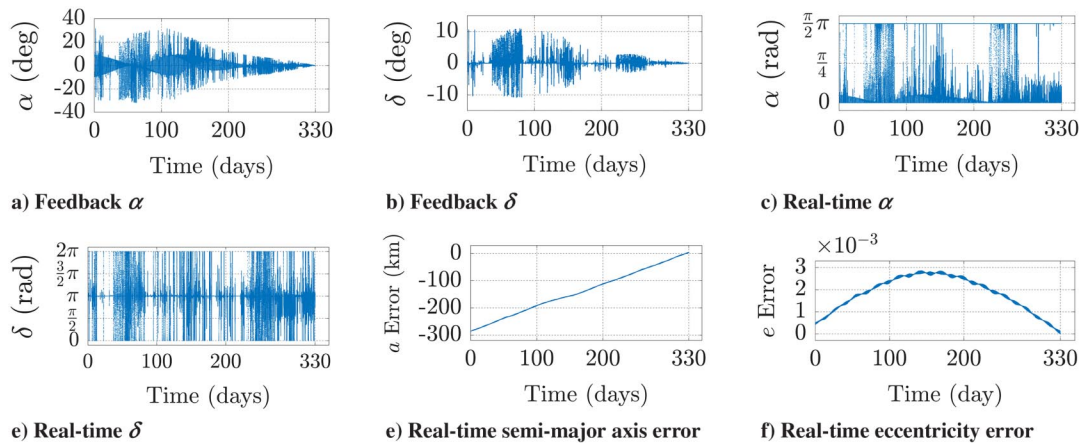


Fig. 6 Optimization using the feedback PS method.

a) Iterative approach I: iterations of linearization

As shown in Fig. 2, we linearize the dynamic system in Eq. (7) along the real-time trajectory generated by the linear feedback controller in the last iteration, and apply another linear feedback controller to further reduce the terminal state error. The penalty matrices in the linear feedback controllers are chosen based on trial and error. In the following set of simulations, the penalty matrices are set to be $S = \text{diag}[1, 10^{11}, 1, 1, 1, 1]$, $Q = \text{diag}[1, 10^6, 1, 1, 1, 1]$, $R = \text{diag}[5 \cdot 10^{14}, 5 \cdot 10^{14}]$. Using the third linear feedback control-

ler, the terminal state error of the semi-major axis and eccentricity are reduced to $+2.8390$ km and $-7.6065 \cdot 10^{-6}$, respectively. As a result, the cost in Eq. (36) is reduced to 3.5997. The optimization history is shown in Fig. 7.

b) Iterative approach II: iterative feedback PS method

As shown in Fig. 2, the real-time control and state trajectory act as the initial guesses for the open-loop PS method in the next iteration, and another linear feedback controller is applied to stabilize the open-loop PS method. In the iterations, the bounds on the states are shrunk

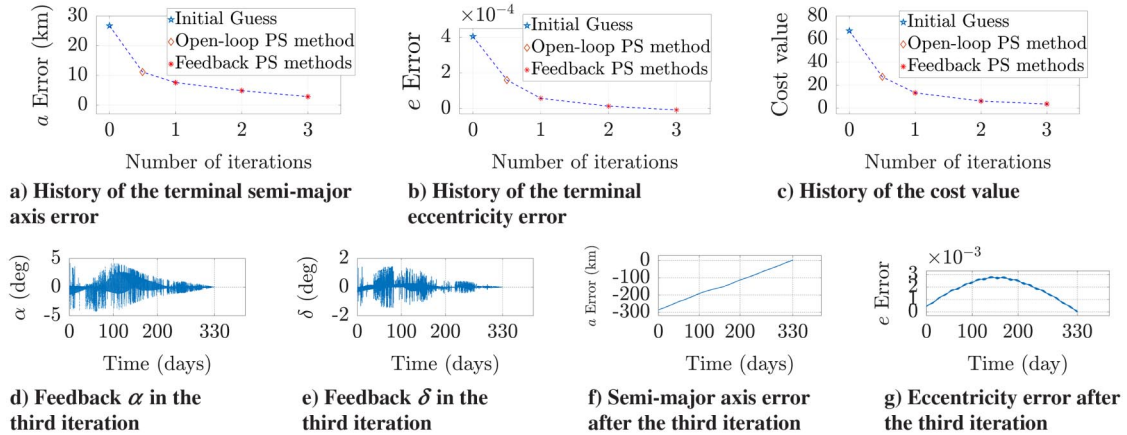


Fig. 7 History of the terminal state error and cost value for each step of optimization, using the iterations of linearization.

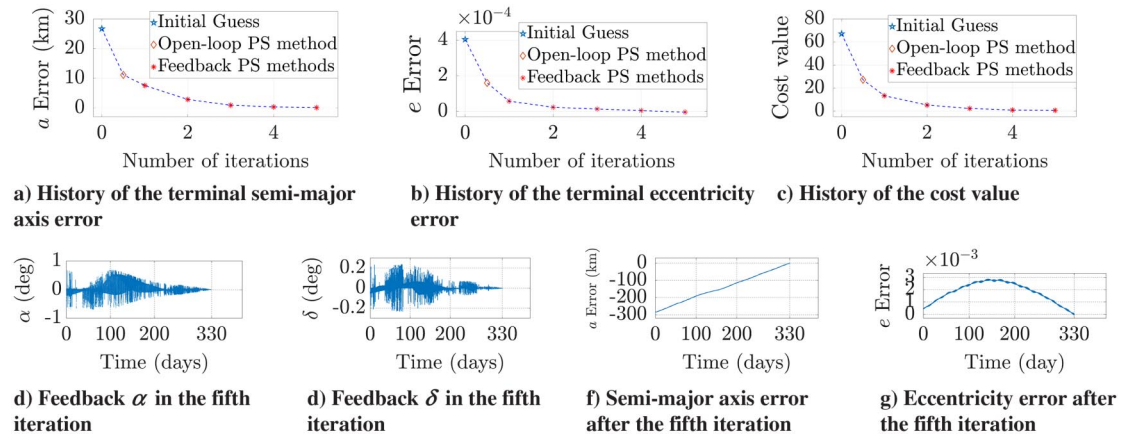


Fig. 8 History of the terminal state error and cost value for each step of optimization, using the iterative feedback PS method.

Table 1 Comparisons between the optimization methods

Optimization method	Accuracy	Computation cost
1. Global LGR PS method [6]	Terminal a error: — Terminal e error: — Terminal cost: <1	~ 432 nodes/day, $\sim 38,880$ nodes in total Global optimization Major optimality/feasibility tolerance: 10^{-6}
2. Linear feedback controller [7]	Terminal a error: $+13.65$ km Terminal e error: $+0.66 \cdot 10^{-3}$ Terminal cost: 79.65	Linear feedback control $\times 1$ Time cost: ~ 55 min
3. Local LGL PS method	Terminal a error: $+11.14$ km Terminal e error: $+1.60 \cdot 10^{-4}$ Terminal cost: 27.16	20 nodes/segment, 60 nodes/day Major optimality/feasibility tolerance: 10^{-5} Time cost: $\sim 3,600$ min
4. Feedback PS method, iteration I	Terminal a error: $+2.83$ km Terminal e error: $-7.60 \cdot 10^{-6}$ Terminal cost: 3.59	Local LGL PS optimization $\times 1$ Linear feedback control $\times 3$ Time cost: $\sim 3,765$ min
5. Feedback PS method, iteration II	Terminal a error: $+0.09$ km Terminal e error: $-4.09 \cdot 10^{-6}$ Terminal cost: 0.49	Local LGL PS optimization $\times 5$ Linear feedback control $\times 5$ Time cost: $\sim 18,275$ min

The optimization methods 2–5 use an Intel i5-9600 K 3.70 GHz CPU, 48.0 GB RAM desktop for calculation.

in each step of the open-loop PS optimization, and the penalty matrices in the linear feedback controllers are chosen based on trial and error. Using the iterative feedback PS method, the terminal state error of the semi-major axis and eccentricity are gradually reduced, and finally to $+0.0903$ km and $-4.0962 \cdot 10^{-6}$, respectively. As a result, the cost in Eq. (36) is reduced to 0.4999. The optimization history is shown in Fig. 8.

C. Comparisons

Table I shows the comparisons between the control approaches applied in [6,7], the local LGL PS method, and the feedback PS method proposed in this work. Compared with the global LGR PS method applied in [6], the proposed feedback PS method requires far fewer nodes, thus costing far less computational time. By using the iterations of the open-loop PS methods and the linear feedback controllers, the proposed feedback PS method greatly improves the optimization accuracy of the linear feedback controller applied in [7] and the local LGL PS method. Within the proposed feedback PS methods, the iterative approach II shows better optimization accuracy, but costs much longer computational time.

V. Conclusions

This Note proposes a feedback PS method for solving nonconvex nonlinear optimal control problems. The feedback is achieved by linearizing the dynamic system along the locally optimal state trajectory generated by the open-loop PS method, then developing a linear feedback controller to stabilize the open-loop PS method. The proposed feedback PS method is particularly useful when it is difficult to find an effective initial guess for the open-loop PS method. The proposed feedback PS method is applied to the removal of end-of-life GEO satellites to the GEO graveyard region using solar sailing. Simulations indicate that end-of-life GEO satellites are successfully removed to the GEO graveyard region using the proposed feedback PS method, and the terminal state error of the semi-major axis and eccentricity are reduced to 0.0903 km and $-4.0962 \cdot 10^{-6}$, respectively.

Acknowledgments

This work is partially supported by the China Scholarship Council (student number 201706230379). The authors want to thank Flora Mei, who offered lots of help in debugging the codes.

References

- [1] Anderson, P. V., and Schaub, H., "Local Debris Congestion in the Geosynchronous Environment with Population Augmentation," *Acta Astronautica*, Vol. 94, No. 2, 2014, pp. 619–628. <https://doi.org/10.1016/j.actaastro.2013.08.023>
- [2] "Classification of Geosynchronous Objects. Issue 20, Revision 0. May 2018. ESA," European Space Agency, 2018, http://www.astronomer.ru/data/0128/Classification_of_Geosynchronous_Objects_I20R0.pdf.
- [3] "Inter-Agency Space Debris Coordination Committee. Space Debris Mitigation Guidelines, Revision 1, September 2007, iadc," Inter-Agency Space Debris Coordination Committee, 2007, http://www.unoosa.org/documents/pdf/spacelaw/sd/IADC-2002-01-IADC-Space_Debris-Guidelines-Revision1.pdf.
- [4] Kelly, P. W., Bevilacqua, R., Mazal, L., and Erwin, R. S., "TugSat: Removing Space Debris from Geostationary Orbits Using Solar Sails," *Journal of Spacecraft and Rockets*, Vol. 55, No. 2, 2018, pp. 437–450. <https://doi.org/10.2514/1.a33872>
- [5] Kelly, P., and Bevilacqua, R., "An Optimized Analytical Solution for Geostationary Debris Removal Using Solar Sails," *Acta Astronautica*, Vol. 162, Sep. 2019, pp. 72–86. <https://doi.org/10.1016/j.actaastro.2019.05.055>
- [6] Kelly, P., and Bevilacqua, R., "Geostationary Debris Mitigation Using Minimum Time Solar Sail Trajectories with Eclipse Constraints," *Optimal Control Applications and Methods*, Vol. 42, No. 1, 2021, pp. 279–304. <https://doi.org/10.1002/oca.2676>
- [7] Mei, H., Damaren, C. J., and Zhan, X., "Hybrid Removal of End-of-Life Geosynchronous Satellites Using Solar Radiation Pressure and Impulsive Thrusts," *Advances in Space Research*, Vol. 66, No. 4, 2020, pp. 974–991. <https://doi.org/10.1016/j.asr.2020.04.052>
- [8] Mei, H., Damaren, C. J., and Zhan, X., "End-of-Life Geostationary Satellite Removal Using Realistic Flat Solar Sails," *Aerospace Systems*, Vol. 4, April 2021, pp. 227–238. <https://doi.org/10.1007/s42401-021-00089-8>
- [9] Conway, B. A., "A Survey of Methods Available for the Numerical Optimization of Continuous Dynamic Systems," *Journal of Optimization Theory and Applications*, Vol. 152, No. 2, 2012, pp. 271–306. <https://doi.org/10.1007/s10957-011-9918-z>
- [10] Ross, I. M., and Fahroo, F., "Legendre Pseudospectral Approximations of Optimal Control Problems," *New Trends in Nonlinear Dynamics and Control and Their Applications*, Springer, Berlin, Heidelberg, 2003, pp. 327–342. https://doi.org/10.1007/978-3-540-45056-6_21
- [11] Benson, D. A., Huntington, G. T., Thorvaldsen, T. P., and Rao, A. V., "Direct Trajectory Optimization and Costate Estimation via an Orthogonal Collocation Method," *Journal of Guidance, Control, and Dynamics*, Vol. 29, No. 6, 2006, pp. 1435–1440. <https://doi.org/10.2514/6.2006-6358>
- [12] Elnagar, G., Kazemi, M. A., and Razzaghi, M., "The Pseudospectral Legendre Method for Discretizing Optimal Control Problems," *IEEE Transactions on Automatic Control*, Vol. 40, No. 10, 1995, pp. 1793–1796. <https://doi.org/10.1109/9.467672>
- [13] Fahroo, F., and Ross, I. M., "Costate Estimation by a Legendre Pseudospectral Method," *Journal of Guidance, Control, and Dynamics*, Vol. 24, No. 2, 2001, pp. 270–277. <https://doi.org/10.2514/6.1998-4222>
- [14] Garg, D., Patterson, M. A., Francolin, C., Darby, C. L., Huntington, G. T., Hager, W. W., and Rao, A. V., "Direct Trajectory Optimization and Costate Estimation of Finite-Horizon and Infinite-Horizon Optimal Control Problems Using a Radau Pseudospectral Method," *Computational Optimization and Applications*, Vol. 49, No. 2, 2011, pp. 335–358. <https://doi.org/10.1007/s10589-009-9291-0>
- [15] Huntington, G., Benson, D., and Rao, A., "A Comparison of Accuracy and Computational Efficiency of Three Pseudospectral Methods," *AIAA Guidance, Navigation and Control Conference and Exhibit*, AIAA Paper 2007-6405, 2007. <https://doi.org/10.2514/6.2007-6405>
- [16] Garg, D., Patterson, M., Hager, W. W., Rao, A. V., Benson, D. A., and Huntington, G. T., "A Unified Framework for the Numerical Solution of Optimal Control Problems Using Pseudospectral Methods," *Automatica*, Vol. 46, No. 11, 2010, pp. 1843–1851. <https://doi.org/10.1016/j.automatica.2010.06.048>
- [17] Fahroo, F., and Ross, I. M., "Advances in Pseudospectral Methods for Optimal Control," *AIAA Guidance, Navigation and Control Conference and Exhibit*, AIAA Paper 2008-7309, 2008. <https://doi.org/10.2514/6.2008-7309>
- [18] Gong, Q., Ross, I. M., Kang, W., and Fahroo, F., "On the Pseudospectral Covector Mapping Theorem for Nonlinear Optimal Control," *Proceedings of the 45th IEEE Conference on Decision and Control*, Inst. of Electrical and Electronics Engineers, New York, 2006, pp. 2679–2686. <https://doi.org/10.1109/cdc.2006.377729>
- [19] Ross, I. M., and Fahroo, F., "A Pseudospectral Transformation of the Convectors of Optimal Control Systems," *IFAC Proceedings Volumes*, Vol. 34, No. 13, 2001, pp. 543–548. [https://doi.org/10.1016/s1474-6670\(17\)39048-1](https://doi.org/10.1016/s1474-6670(17)39048-1)
- [20] Williams, P., "Hermite-Legendre-Gauss-Lobatto Direct Transcription in Trajectory Optimization," *Journal of Guidance, Control, and Dynamics*, Vol. 32, No. 4, 2009, pp. 1392–1395. <https://doi.org/10.2514/1.42731>
- [21] Rao, A. V., "A Survey of Numerical Methods for Optimal Control," *Advances in the Astronautical Sciences*, Vol. 135, No. 1, 2009, pp. 497–528.
- [22] Huntington, G. T., and Rao, A. V., "Comparison of Global and Local Collocation Methods for Optimal Control," *Journal of Guidance, Control, and Dynamics*, Vol. 31, No. 2, 2008, pp. 432–436. <https://doi.org/10.2514/1.30915>
- [23] Narayanaswamy, S., and Damaren, C. J., "Comparison of the Legendre-Gauss Pseudospectral and Hermite-Legendre-Gauss-Lobatto Methods for Low-Thrust Spacecraft Trajectory Optimization," *Aerospace Systems*, Vol. 3, Jan. 2020, pp. 53–70. <https://doi.org/10.1007/s42401-019-00042-w>
- [24] Ross, I., Sekhvat, P., Fleming, A., Gong, Q., and Kang, W., "Pseudospectral Feedback Control: Foundations, Examples and Experimental Results," *AIAA Guidance, Navigation, and Control Conference and Exhibit*, AIAA Paper 2006-6354, 2006. <https://doi.org/10.2514/6.2006-6354>
- [25] Bollino, K. P., and Ross, I. M., "A Pseudospectral Feedback Method for Real-Time Optimal Guidance of Reentry Vehicles," *2007 American*

- Control Conference*, Inst. of Electrical and Electronics Engineers, New York, 2007, pp. 3861–3867.
<https://doi.org/10.1109/ACC.2007.4282500>
- [26] Yan, H., Ross, I. M., and Alfriend, K. T., “Pseudospectral Feedback Control for Three-Axis Magnetic Attitude Stabilization in Elliptic Orbits,” *Journal of Guidance, Control, and Dynamics*, Vol. 30, No. 4, 2007, pp. 1107–1115.
<https://doi.org/10.2514/1.26591>
- [27] Vallado, D. A., *Fundamentals of Astrodynamics and Applications*, Vol. 12, Springer Science & Business Media, Berlin, 2001, Chap. 8.
- [28] McInnes, C. R., *Solar Sailing: Technology, Dynamics and Mission Applications*, Springer Science & Business Media, Berlin, 2004, Chap. 2.
- [29] Bryson, A. E., and Ho, Y.-C., *Applied Optimal Control: Optimization, Estimation, and Control*, Routledge, Oxfordshire, England, U.K., 2018, Chap. 6.
- [30] Gill, P. E., Murray, W., and Saunders, M. A., “SNOPT: An SQP Algorithm for Large-Scale Constrained Optimization,” *SIAM Review*, Vol. 47, No. 1, 2005, pp. 99–131.
<https://doi.org/10.1137/s0036144504446096>